

## Isatin-Derived Compounds as Carbon Steel Corrosion Inhibitors in Highly Saline Media

A. B. da Silva<sup>1</sup>, J. A. C. P. Gomes<sup>1,\*</sup>, E. D'Elia<sup>2</sup>, M. J. C. Rezende<sup>2</sup>, A. C. Pinto<sup>2</sup>, B. N. M. Silva<sup>2</sup>,  
B. V. Silva<sup>2</sup>

<sup>1</sup> Laboratório de Corrosão, Programa de Engenharia Metalúrgica e de Materiais, COPPE, Universidade Federal do Rio de Janeiro, Ilha do Fundão, Centro de Tecnologia, Rio de Janeiro, RJ, Brazil.

<sup>2</sup> Instituto de Química, UFRJ Avenida Athos da Silveira Ramos 149, Centro de Tecnologia, Bloco A, CEP 21941-909, Cidade Universitária, Rio de Janeiro - RJ, Brazil.

\*E-mail: [ponciano@metalmat.ufrj.br](mailto:ponciano@metalmat.ufrj.br)

Received: 8 April 2013 / Accepted: 13 June 2013 / Published: 1 July 2013

---

Carbon steel corrosion in CO<sub>2</sub>-saturated solutions, simulating the produced water generated in oil and gas extraction, was investigated using weight loss, electrochemical measurements and surface characterization. The effectiveness of two isatin compounds, *N*-morpholine-isatin (MI) and *N*-morpholine-3-isatin-thiosemicarbazone (MIT) as corrosion inhibitors in these highly saline media was also evaluated. Only MIT was shown to act as a corrosion inhibitor for carbon steel immersed in both of the simulated produced water solutions evaluated. The impedance results corroborated the corrosion mechanisms commonly accepted in the literature.

---

**Keywords:** carbon steel; CO<sub>2</sub> corrosion; chloride media; corrosion inhibitor; isatin.

### 1. INTRODUCTION

Carbon steel corrosion is a common problem in the petroleum industry. Produced water, a saline medium generated during oil production, is considered the most corrosive environment in oil field operations due to the presence of aggressive corrosive agents, such as chloride and sulfate ions, and gases, such as carbon dioxide (CO<sub>2</sub>) and hydrogen sulfide (H<sub>2</sub>S). CO<sub>2</sub> dissolves in water, creating a weak acid, carbonic acid, which can severely corrode the steel pipelines and equipment used in the production and transportation of oil and gas. Cations, such as sodium (Na<sup>+</sup>), potassium (K<sup>+</sup>), calcium (Ca<sup>2+</sup>), magnesium (Mg<sup>2+</sup>), barium (Ba<sup>2+</sup>), and strontium (Sr<sup>2+</sup>), and anions, such as sulfate (SO<sub>4</sub><sup>2-</sup>), carbonate (CO<sub>3</sub><sup>2-</sup>) and bicarbonate (HCO<sub>3</sub><sup>-</sup>), can also affect the buffering capacity, salinity and scale potential of the produced water [1]. The injection of corrosion inhibitors has been an effective and

flexible way to control these factors and processes. Well-known inhibitors include imidazolines, amines and amides. Imidazoline-derived compounds are considered the most effective, and therefore most used, corrosion inhibitors [2, 3].

Many studies have simulated CO<sub>2</sub> corrosion of steel in saline media with chloride levels up to 30,000 mg L<sup>-1</sup> [3, 7-10]. However, increased exploratory drilling and production at high depths than 2400 m present complex corrosion problems due to the variable CO<sub>2</sub> concentrations and the high-salinity and high-pressure corrosive environment present [11-13].

The corrosive processes in these highly saline environments are not completely understood. Few studies have focused on highly saline media with chloride concentrations greater than 100,000 mg L<sup>-1</sup> that also contain cations such as Ca<sup>2+</sup> and Mg<sup>2+</sup> [2, 4, 14, 15]. These cations may cause scale deposition and influence the susceptibility to pitting and/or uniform corrosion [16]. Some researchers have studied aerated saline media containing chloride concentrations of approximately 132,000 mg L<sup>-1</sup>, with Ca<sup>2+</sup>, SO<sub>4</sub><sup>2-</sup>, Mg<sup>2+</sup> and surfactants as inhibitors [4].

The aim of this paper is to investigate carbon steel corrosion in CO<sub>2</sub>-saturated, highly saline solutions that simulate real-world aqueous media using electrochemical techniques, weight loss measurements and surface characterization. The effectiveness of *N*-morpholine-isatin (MI) and *N*-morpholine-3-isatin-thiosemicarbazone (MIT) as corrosion inhibitors will also be evaluated. These inhibitors were selected because isatin- and semicarbazone-derived compounds contain  $\pi$ -electrons and heteroatoms such as N, O and S, which may promote greater adsorption of the inhibitor molecules onto steel surfaces [14]. These compounds have wide applications in chemistry [17]. Some authors have shown isatin-, semicarbazone- and thiosemicarbazone-derived compounds to be effective corrosion inhibitors for aluminum, copper and steel in hydrochloric, nitric and sulfuric acid solutions [18, 19]. The effects of thiosemicarbazone compounds on carbon steel corrosion in sodium chloride solutions containing dissolved H<sub>2</sub>S have also been studied [20]. Prior to this paper, there have been no studies on these compounds in highly saline media containing a wide range of cations and anions in addition to sodium chloride salt with CO<sub>2</sub> present. In addition, a comparative study of corrosion in simulated produced water solutions differing in chloride and calcium content will be conducted.

## 2. EXPERIMENTAL

### 2.1. Synthesis of inhibitors

#### *N*-morpholine-isatin (MI)

Isatin (5 mmol) was suspended in a solution of formalin (2 mL) and tetrahydrofuran (5 mL); 5 mmol (0.4 mL) of morpholine was then added dropwise while cooling and stirring. The reaction mixture was magnetically stirred for 1 hour and then gently heated in a water bath for 15 minutes. After this period, the reaction medium was cooled, and the orange precipitate was isolated by vacuum filtration [21]. The yield was 71 %. The chemical structure of *N*-morpholine-isatin is shown in Figure 1. Experimental data: IR  $\nu_{\max}$ (KBr)/cm<sup>-1</sup>: 3461, 3450, 2954, 2856, 1731, 1608 and 1467; <sup>1</sup>H NMR  $\delta_{\text{H}}$  (200 MHz, CDCl<sub>3</sub> + DMSO): 7.63 (1H, td, *J* 1 and 8 Hz), 7.53 (1H, dd, *J* 1 and 8 Hz), 7.25 (1H, dd, *J*

1 and 8Hz), 7.12 (1H, td,  $J$  1 and 8 Hz), 4.38 (2H, s), 3.54 (4H, m), 2.55 (4H, m),  $^{13}\text{C}$  NMR  $\delta_{\text{C}}$  (50 MHz,  $\text{CDCl}_3 + \text{DMSO}$ ): 183, 159, 151, 138, 124, 123, 117, 112, 66, 61, 50.

#### *N*-morpholine-3-isatin-thiosemicarbazone (MIT)

Thiosemicarbazide (20 mmol) and isatin (20 mmol) were suspended in 100 mL of methanol. The reaction mixture was stirred magnetically under reflux for 1 hour. Afterward, the yellow precipitate, isatin-3-thiosemicarbazone, was filtered out under vacuum and dried at room temperature. The synthesized isatin-3-thiosemicarbazone (3 mmol) was suspended in a solution of formalin (2.0 mL) and THF (5.0 mL); 5 mmol (0.4 mL) of morpholine was then added dropwise while cooling and stirring. The reaction mixture was magnetically stirred for 2 hours. The yellow precipitate formed was then isolated by vacuum filtration. [22]. The yield was 71 %. The chemical structure of this compound is shown in Figure 1. Experimental data: IR  $\nu_{\text{max}}$ (KBr)/ $\text{cm}^{-1}$ : 3393, 3171, 2966, 1715, 1686, 1616 and 1607;  $^1\text{H}$  NMR  $\delta_{\text{H}}$  (200 MHz,  $\text{CDCl}_3 + \text{DMSO}$ ): 12.4 (1H, s), 9.1 (1H, s), 7.6-7.9 (1H, m), 7.4-7.1(3H, m), 4.5 (2H, br s), 3.5 (4H, br s), 2.5 (4H, br s),  $^{13}\text{C}$ NMR  $\delta_{\text{C}}$  (50 MHz,  $\text{CDCl}_3 + \text{DMSO}$ ): 179, 162, 144, 131, 123, 121, 120, 111, 66, 61, 51.

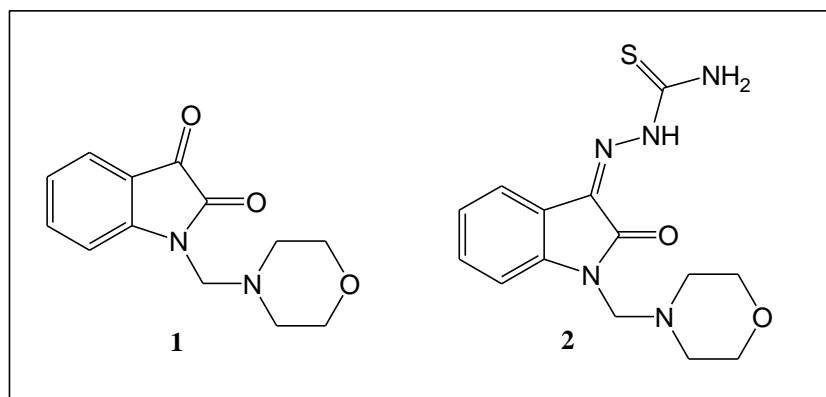


**Figure 1.** Chemical structures of the isatin derived compounds: (1) *N*-morpholine-isatin (MI) and (2) *N*-morpholine-3-isatin-thiosemicarbazone (MIT).

#### 2.2. Solutions

Two test solutions were prepared from different analytical-grade chemical reagents dissolved in distilled water, simulating produced water. The chemical compositions of the two synthetic solutions,  $W_1$  and  $W_2$ , are listed in Table 1. The solutions were saturated with  $\text{CO}_2$  for one hour prior to any immersion of the carbon steel specimens or addition of the inhibitors. The gas was continuously supplied to the solution to ensure total saturation during the measurements. The inhibitors used have very low water solubility and therefore were dissolved in ethanol, at 2 % (v/v), before being added to the simulated water. The maximum inhibitor concentrations were  $30 \text{ mg L}^{-1}$  for MI and  $4 \text{ mg L}^{-1}$  for MIT. The inhibitors were added to the  $\text{CO}_2$ -saturated solution and the pH measured immediately before immersing the metal specimen. It is important to mention that the inhibitor concentrations cited

in this study are the saturation concentrations in 2 % (v/v) ethanol/simulated produced water. The blank solution consisted of simulated produced water containing 2 % (v/v) ethanol.

**Table 1.** Simulated produced water solutions compositions.

Composition	Concentration (mg L <sup>-1</sup> )	
	W <sub>1</sub>	W <sub>2</sub>
Na <sup>+</sup>	89435	72209
K <sup>+</sup>	3955	1733
Mg <sup>++</sup>	1184	757
Ca <sup>++</sup>	14485	2350
Ba <sup>++</sup>	22	20
Sr <sup>++</sup>	1509	380
Cl <sup>-</sup>	171400	115000
SO <sub>4</sub> <sup>2-</sup>	340	62
HCO <sub>3</sub> <sup>-</sup>	386	1232
CH <sub>3</sub> COOH	-	227

### 2.3. Weight loss measurements

Rectangular carbon steel specimens with dimensions 25 x 25 x 1 mm were prepared from steel of the following chemical composition: C 0.075 %, P 0.025 %, Mn 0.52 %, Cr 0.06 %, Ni, 0.06 % and Fe 98.9 %. The specimens were mechanically abraded with emery paper starting at 300 and terminating at 600 grit, cleaned with ethanol, dried in hot air and, finally, weighed on a balance with 0.1 mg precision. The tests were performed according to ASTM practice standard G-31 [23]. Corrosion rates (CRs) were determined after 24 hours of immersion in the simulated water solutions. After the experiment, samples were chemically treated to remove all corrosion products. Clark solution, consisting of 1000 mL of hydrochloric acid, 20 g of antimony trioxide (Sb<sub>2</sub>O<sub>3</sub>) and 50 g of stannous chloride (SnCl<sub>2</sub>), was prepared according to ASTM practice standard G-1 [24]. The specimens were immersed in this solution for 40 seconds, rinsed with water, cleaned with ethanol in an ultrasonic bath for 10 minutes, dried in hot air and, finally, weighed. Three identical specimens were processed in each experiment. The standard deviation of the measurements was approximately 0.001 mm/year. The mean value was reported and used for further data processing. The corrosion rate (mm/year) was calculated following the equation in ASTM practice standard G-31 [23].

### 2.4. Electrochemical measurements

Open circuit potential (OCP), polarization curve and electrochemical impedance spectroscopy (EIS) measurements were performed using a conventional three-electrode glass cell, with an approximately 1 cm<sup>2</sup> surface area carbon steel working electrode (WE), a platinum wire counter electrode (CE) and a saturated calomel electrode (SCE) as the reference. Prior to all measurements, the

carbon steel electrode, which had the same composition as the weight-loss measurement specimens, was mechanically abraded with emery paper progressing from 300 to 600 grit, cleaned with ethanol and finally dried in hot air. All polarization curve and EIS measurements were carried out using an Autolab digital potentiostat, model PGSTAT 302, with the GPES and FRA software, respectively.

First, the working electrode was immersed in the solution for 1 hour to achieve a steady OCP. After the OCP was determined, EIS measurements were performed in a frequency range of 10 KHz to 2 mHz with a sinusoidal signal amplitude of 10 mV. Potentiodynamic cathodic and anodic polarization curves were recorded from the corrosion potential to 300 mV of cathodic and anodic overpotential at a scan rate of 20 mV min<sup>-1</sup>. All experiments were performed at atmospheric pressure and ambient temperature in a CO<sub>2</sub>-saturated solution and performed at least twice to ensure repeatability.

### 2.5. Surface characterization

Scanning electron microscopy (SEM) was used to study the surface morphology of carbon steel after exposure to produced water. The microscope used was a JEOL JSM6460LV operating at 20 kV in secondary electron imaging mode. Carbon steel specimens with a 15 cm<sup>2</sup> surface area were mechanically abraded with emery paper progressing from 300 to 600 grit, cleaned with ethanol and, finally, dried in hot air. After 24 h of immersion, the specimens were gently washed with distilled water and then cleaned in ethanol for 10 minutes in an ultrasonic bath to remove any corrosion products and avoid salt crystallization from the highly saline solution prior to imaging. All micrographs of the corroded carbon steel specimens were taken at a magnification of 2000x.

## 3. RESULTS AND DISCUSSION

### 3.1. pH measurements

**Table 2.** pH values of CO<sub>2</sub>-saturated simulated produced water with and without the isatin-derived inhibitors MI and MIT.

Solution	pH	
	W <sub>1</sub>	W <sub>2</sub>
Blank	4.79	5.30
MI	4.78	5.40
MIT	4.75	5.41

Table 2 presents pH values of the CO<sub>2</sub>-saturated produced water solutions with and without the isatin-derived compounds. pH measurements were performed immediately prior to the immersion of the carbon steel specimens for the weight loss and electrochemical measurements. It can be seen that W<sub>1</sub> was more acidic than W<sub>2</sub>, most likely due to the higher bicarbonate ion content in W<sub>2</sub>. There was no significant pH variation in either saline medium after the addition of MI or MIT. A constant pH after the addition of inhibitors is important for avoiding scale formation, once a pH increase can induce CaCO<sub>3</sub> precipitation [25].

### 3.2. Weight loss measurements

Table 3 shows the corrosion rate (CR) of carbon steel specimens after 24 hours of immersion in the CO<sub>2</sub>-saturated simulated produced water solutions W<sub>1</sub> and W<sub>2</sub>, with and without MI and MIT. The CR was calculated from weight-loss measurement data. The CRs obtained for W<sub>2</sub> were higher than those for W<sub>1</sub>. In both simulated produced water solutions, the presence of MI increased the CR. In contrast, the addition of MIT reduced the CR in both produced water solutions.

**Table 3.** Weight-loss data for carbon steel immersed in CO<sub>2</sub>-saturated simulated produced water solutions with and without the corrosion inhibitors, MI and MIT.

Solution	Concentration (mg L <sup>-1</sup> )	CR <sub>W1</sub> (mm/year)	IE <sub>W1</sub> (%)	CR <sub>W2</sub> (mm/year)	IE <sub>W2</sub> (%)
Blank	*	0.0955	*	0.1278	*
MI	30	0.0978	-2	0.1369	-7
MIT	4	0.0139	85	0.0170	87

The inhibition efficiencies (IE %) were calculated from the CRs and are presented in Table 3. The values were calculated according to equation (1):

$$IE (\%) = [(CR_0 - CR_i) / CR_0] \times 100, \quad (1)$$

where  $CR_0$  and  $CR_i$  are the corrosion rates of carbon steel in the absence and presence of the inhibitor, respectively.

According to these results, for both saline media evaluated, only MIT was an effective carbon steel corrosion inhibitor. MIT presented an IE of 85 % for W<sub>1</sub> and 87 % for W<sub>2</sub>. The presence of MI caused an increase in the CR, resulting in negative IE values.

The CRs obtained for the second produced water solution (W<sub>2</sub>), in both the absence and presence of MI and MIT, were higher than those of the first, indicating that W<sub>1</sub> was less corrosive despite being more acidic (Table 2) and containing more chloride (Table 1) and therefore being considered potentially more corrosive. This reversal indicates that the concentrations and presence of other ions play an important role in the corrosive processes occurring. The formation of corrosion products, films and scale, caused by Ca<sup>2+</sup> and Mg<sup>2+</sup> ions for example, can potentially interfere with the corrosion process through the formation of protective films. Some studies have found that Cl<sup>-</sup> and Ca<sup>2+</sup> can influence the corrosion rate of carbon steel in sodium chloride solutions. Jiang *et al.* [16] showed that the corrosion rate increased with increased Cl<sup>-</sup> concentration and that for solutions with identical Cl<sup>-</sup> concentrations, the corrosion rate decreased with the addition of Ca<sup>2+</sup>. They associated this phenomenon with the formation of a thick scale composed of CaCO<sub>3</sub>, FeCO<sub>3</sub>, and Fe<sub>3</sub>C, which provided corrosion protection by decreasing the transport rate of reactive species to the metal surface. The protective performance of carbonate, sulfate or oxide, however, may depend on the characteristics of the scale formed [26]. Sun *et al.* [27] mentioned the formation of a thin, porous non-protective FeCO<sub>3</sub> scale. HCO<sub>3</sub><sup>-</sup> concentration may also influence the carbon steel corrosion process in saline media. Some authors observed a reduced corrosion rate with increasing HCO<sub>3</sub><sup>-</sup> concentration and the

formation of carbonates of Fe, Ca and Mg [30, 31]. It is evident that the solutions evaluated in this work have complex carbon steel corrosion processes due to the presence of many ions that can interfere with the process in different manners.

It was observed that in both  $W_1$  and  $W_2$ , the presence of MI produced a higher CR than that of the blank solution and, consequently, negative IEs. There is little information about this behavior in literature. López *et al.* [30] recorded similar results for carbon steel corrosion in a  $CO_2$ -saturated sodium chloride 5 % solution when an imidazoline-derived compound was added. This molecule theoretically protected against steel corrosion, having nitrogen atoms as electron donors while  $Fe^{2+}$  ions and metallic Fe acted as electron acceptors. The detrimental behavior observed was linked to interference with the formation of  $FeCO_3$  protective barriers, and the absence of hydrophobic hydrocarbon chains. Some authors have also suggested that the structure of the inhibitor should interact with the crystal structures of the corrosion products [31].

### 3.3. Electrochemical measurements

#### 3.3.1. OCP measurements

OCPs as a function of time for carbon steel immersed in  $CO_2$ -saturated simulated produced water solutions  $W_1$  and  $W_2$  are shown in Figures 2 A and B. The OCP steadies after 1 hour of carbon steel electrode immersion.

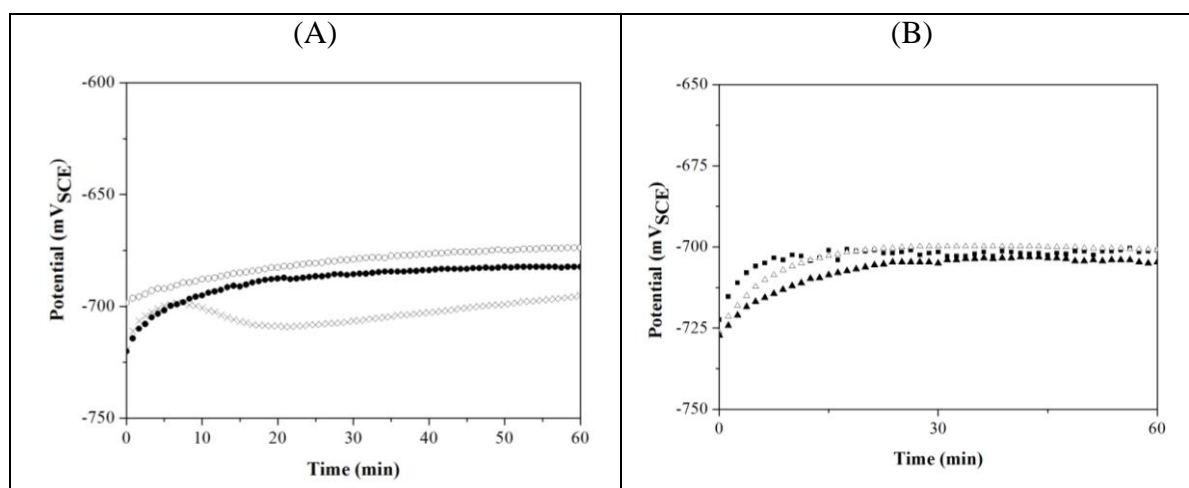


**Figure 2.** OCPs of carbon steel immersed in  $CO_2$ -saturated simulated produced water solutions with and without isatin-based inhibitors, MI and MIT.  $W_1$  (A): (o) blank, (●) MI and (x) MIT;  $W_2$  (B): (Δ) blank, (▲) MI and (■) MIT.

As seen in Table 4, there was no significant variation of the OCP for any of the conditions studied. The OCP remained within the ranges of  $-676$  to  $-690$  mV<sub>SCE</sub> and  $-700$  to  $-704$  mV<sub>SCE</sub> for  $W_1$  and  $W_2$ , respectively.

**Table 4.** OCP values obtained for a carbon steel electrode immersed in CO<sub>2</sub>-saturated simulated produced water solutions with and without the isatin compounds MI and MIT.

Solution	OCP (mV <sub>SCE</sub> )	
	W <sub>1</sub>	W <sub>2</sub>
Blank	-676	-700
MI	-682	-704
MIT	-690	-701

3.3.2. EIS measurements

Electrochemical impedance spectroscopic (EIS) results, obtained at the corrosion potential, for W<sub>1</sub> and W<sub>2</sub> with and without the isatin-derived compounds present are shown in Figures 3 and 4 in Nyquist and Bode diagram format.

The impedance diagram obtained for W<sub>1</sub> in the absence of all inhibitors (Figure 3A) showed two depressed semicircles, attributed to two time constants, one capacitive loop in the high-frequency range followed by a small inductive loop in the low-frequency range.

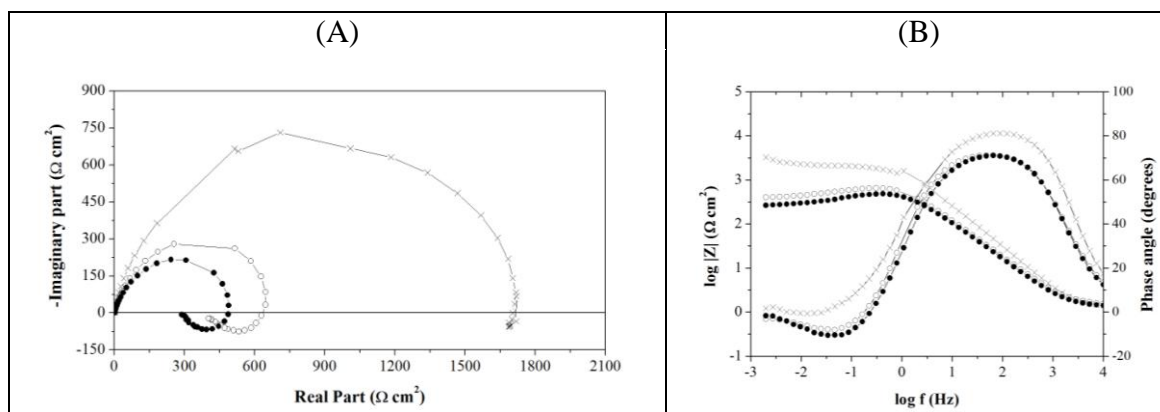


**Figure 3.** Nyquist diagrams and Bode plots obtained at the corrosion potential for carbon steel in CO<sub>2</sub>-saturated simulated produced water, W<sub>1</sub>, in the absence (o) and presence of isatin-derived compounds MI (●) and MIT (x).

The capacitive semicircle obtained in the higher-frequency range could be associated with double-layer capacitance and charge-transfer resistance, while the inductive semicircle at low-frequency is usually related to an adsorbed intermediate species formed during the dissolution of the electrode [32]. This behavior was also observed by others performing EIS studies in CO<sub>2</sub> media [7, 27, 32, 33]. The inductive loop was attributed to active dissolution of the carbon steel, through intermediate species FeOH<sub>ads</sub>, according to equation 2 of the mechanism:





The corresponding Bode plot of phase angle *versus* frequency presented in Figure 3B shows one high-frequency peak at approximately 100 Hz and a low-frequency valley at approximately 47 mHz.

The Nyquist diagram and Bode plots for the MI-containing solution were very similar to those of the blank solution, a capacitive loop in the high-frequency range and a small inductive loop in the low-frequency range. The diameter of the capacitive semicircle in the Nyquist plot was a little smaller than that of the blank solution, showing a lower charge transference resistance ( $R_{ct}$ ).

On the other hand, in the presence of MIT, the impedance response changed. Over all frequency ranges recorded, only a capacitive loop was observed. This loop showed an increase in  $R_{ct}$  suggesting an increase in inhibitor adsorption and reduction of the corrosion process. The corresponding Bode plot showed that the phase angle increased upon addition of MIT. The same trend was observed for the impedance modulus.

The EIS parameters of charge transfer resistance ( $R_{ct}$ ), double-layer capacitance ( $C_{dl}$ ) and IE % were obtained from the Nyquist diagram and are shown in Table 5. The intersection of the semicircle with the real axis at high frequencies occurs at approximately  $1.57 \Omega \text{ cm}^2$ , corresponding to the ohmic resistance of the solution ( $R_s$ ). The first semicircle's intersection with the real axis is  $R_{ct}$ . The  $C_{dl}$  values were calculated at the maximum frequency ( $f_{max}$ ) from the capacitive loop according to equation (2) [4]:

$$C_{dl} = \frac{1}{2\pi f_{max} R_{ct}} \quad (2)$$

The IE results were calculated from  $R_{ct}$  following equation (3):

$$IE(\%) = \left[ 1 - \left( \frac{R_{ct_0}}{R_{ct_i}} \right) \right] \times 100 \quad (3)$$

where  $R_{ct_i}$  and  $R_{ct_0}$  are the polarization resistances obtained with and without the inhibitor present, respectively.

**Table 5.** EIS parameters obtained from Nyquist diagrams for carbon steel in CO<sub>2</sub>-saturated simulated produced water solution, W<sub>1</sub>, in the absence and presence of isatin-derived MI and MIT.

Solution	Concentration (mg L <sup>-1</sup> )	$R_{ct}$ ( $\Omega \text{ cm}^2$ )	$f_{max}$ (Hz)	$C_{dl}$ ( $\mu\text{F cm}^{-2}$ )	IE <sub>W1</sub> (%)
Blank	*	629	2.036	124	*
MI	30	487	2.036	160	-29
MIT	4	1708	2.036	46	63

As seen in Table 5, only MIT acted as a corrosion inhibitor in  $W_1$  exhibiting an IE of 63 %. A decrease in  $C_{dl}$  was also observed with the addition of MIT. The  $R_{ct}$  increase associated with decreased  $C_{dl}$  could be related to inhibitor adsorption [8]. The addition of MI produced a different result: decreased  $R_{ct}$ , resulting in a negative IE.

The Nyquist diagrams and Bode plots obtained for  $W_2$  are presented in Figures 4 A and B. The EIS measurements obtained were different from those for  $W_1$ .

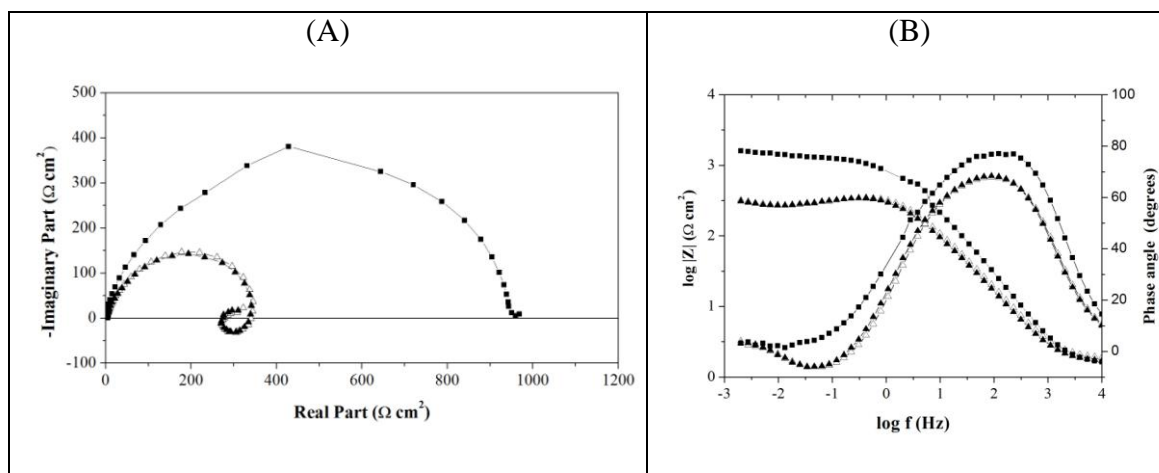


**Figure 4.** Nyquist diagrams and Bode plots obtained at the corrosion potential for carbon steel in  $CO_2$ -saturated produced water,  $W_2$ , in the absence ( $\Delta$ ) and presence of isatin-derived compounds MI ( $\blacktriangle$ ) and MIT ( $\blacksquare$ ).

As seen in Figure 4A, in the absence of organic inhibitors, the Nyquist diagram contains three semicircles that can be attributed to three time constants. There is one capacitive semicircle in the high-frequency range, followed by an inductive semicircle and another low-frequency range capacitive semicircle. It should be noted that only the initial part of the third semicircle is observed in both the Nyquist diagram and Bode plot due to the low-frequency of this final relaxation process. In the Bode plot of phase angle *versus* log frequency, three time constants can be seen, one peak in the high-frequency range followed by a valley and another peak in the low-frequency range.

The appearance of this new capacitive semicircle in the low-frequency range could be related to the formation of corrosion scale ( $FeCO_3$ ) on the electrode surface. Some investigations have demonstrated such a formation on steel in  $CO_2$ -containing solutions [27, 32, 34]. Zhang *et al.* [32] developed a mechanistic model to illustrate corrosion scale electrochemical formation including the dissolution of Fe by bicarbonate ions (reaction 4) and/or precipitate produced from  $Fe^{2+}$ , shown in reaction 3 (reaction 5). This model includes the mechanism of  $FeOH_{ads}$  formation previously shown (reactions 1-3) and the formation of  $FeCO_3$  scale as follows (reactions 4-5):



Two different behaviors were observed with the addition of the organic inhibitors. The results obtained with MI present were similar to those obtained for the blank solution. The Nyquist diagrams (Figure 4A) showed three semicircles: one capacitive at high frequencies, followed by an inductive and another that was capacitive at low frequencies. Analysis of the Bode plot in Figure 4B showed that the phase angle and impedance modulus presented the same trend as for the blank solution. In the phase angle *versus* log frequency plot, a peak in the high-frequency range, a valley in the middle-frequency range and a third peak in the low-frequency range is observed. With MIT present, however, the Nyquist diagram shows only one capacitive semicircle for the whole frequency range examined. The Bode plot of phase angle vs. frequency shows one peak for the entire frequency range. An increase in the impedance modulus can also be observed in the Bode plots (Figure 4B) when MIT is present.

The EIS parameters  $R_{ct}$ ,  $C_{dl}$  and IE were calculated as previously described and shown in Table 6. The ohmic resistance of the solution ( $R_s$ ) was approximately  $1.7 \Omega \text{ cm}^2$ .

Table 6 shows that in  $W_2$ , as in  $W_1$ , only MIT successfully inhibited carbon steel corrosion with an IE of 65 %. Again, the addition of MI resulted in a  $R_{ct}$  smaller than that for the blank solution, resulting in a negative IE, indicating increased corrosion. Additionally, compared to the blank solution, a higher  $R_{ct}$  and smaller  $C_{dl}$  were observed when MIT was present, indicating inhibition adsorption [8]. It is important to mention that for MI, the IE values calculated from the electrochemical measurements corroborated the negative IE values from the weight loss measurements, indicating a corrosion-activation effect caused by the presence of MI.

**Table 6.** EIS parameters obtained from the Nyquist diagram and Bode plot for carbon steel in  $\text{CO}_2$ -saturated produced water,  $W_2$ , in the absence and presence of isatin-derived compounds MI and MIT.

Solution	Concentration ( $\text{mg L}^{-1}$ )	$R_{ct}$ ( $\Omega \text{ cm}^2$ )	$f_{\max}$ (Hz)	$C_{dl}$ ( $\mu\text{F cm}^{-2}$ )	$\text{EI}_{W_2}$ (%)
Blank	*	338	2.79	168	*
MI	30	367	2.036	213	-8
MIT	4	958	2.036	81	65

It was also observed that the  $R_{ct}$  obtained for carbon steel immersed in  $W_2$  ( $338 \Omega \text{ cm}^2$ ) was lower than that obtained for  $W_1$  ( $629 \Omega \text{ cm}^2$ ), indicating that  $W_2$  is more corrosive. This finding agrees with the weight loss results. Although some authors have indicated that  $\text{FeCO}_3$  scale formed a protective barrier, the results obtained in the present work show the opposite behavior [28, 29]. There may have been insufficient  $\text{FeCO}_3$  present to reduce the carbon steel corrosion rate. Although porous and non-protective  $\text{FeCO}_3$  scale formation may influence the results presented in this work, some authors have indicated that the dissolution of iron can be accelerated by dissolution of the carbonate layer promoted by a higher  $\text{HCO}_3^-$  concentration [35, 36]. In these cases, a stable soluble complex anion ( $\text{Fe}(\text{CO}_3)_2^{-2}$ ) formed, as shown in reaction 6 [32]:



### 3.3.3. Potentiodynamic polarization curves

Figure 5 and 6 present the anodic and cathodic polarization curves of carbon steel immersed in the simulated produced water solutions  $W_1$  and  $W_2$ , respectively, in the absence and presence of the isatin-derived compounds MI and MIT. A comparative analysis of these curves showed that only MIT caused a reduction in both the anodic and cathodic current densities. According to Cao [37], the decreasing current without shifts of  $E_{corr}$  could be explained by adsorption of organic compounds, such as the isatin compounds studied here, on the electrode surface, retarding metallic dissolution and the cathodic process and consequently slowing down the corrosion process.

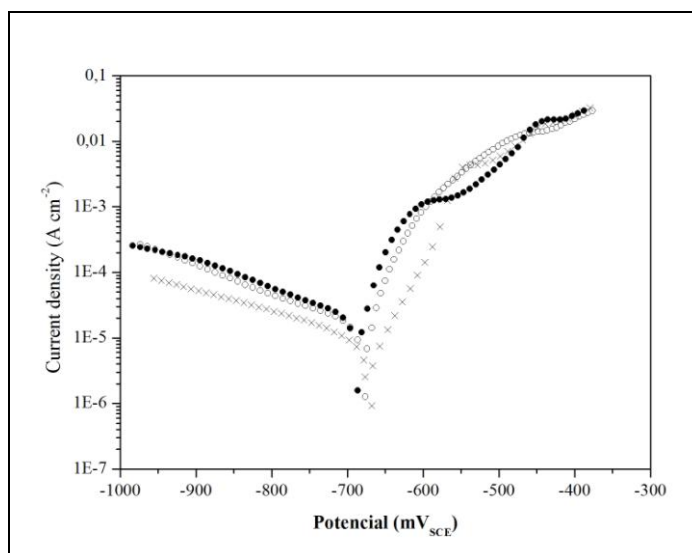


**Figure 5.** Polarization curves of carbon steel in  $CO_2$ -saturated simulated produced water,  $W_1$ , in the absence (o) and presence of isatin-derived compounds MI (●) and MIT (x).

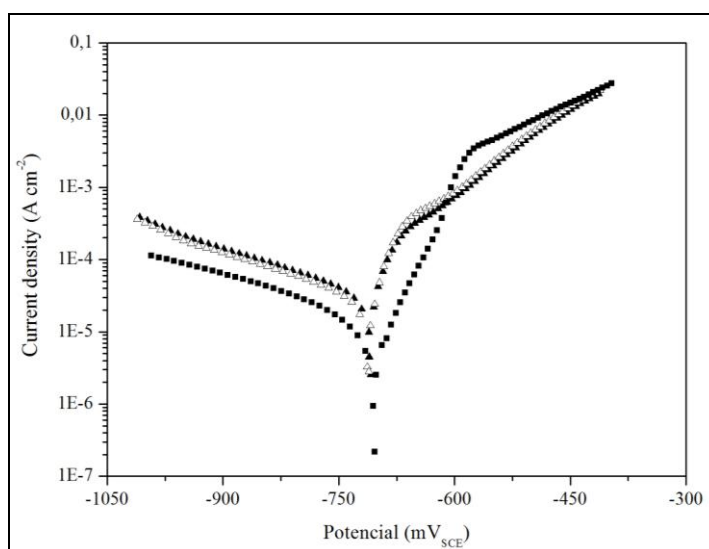


**Figure 6.** Polarization curves of carbon steel in  $CO_2$ -saturated produced water,  $W_2$ , in the absence ( $\Delta$ ) and presence of isatin-derived compounds, MI ( $\blacktriangle$ ) and MIT. ( $\blacksquare$ )

The addition of MI to  $W_1$  generated cathodic and anodic current densities that were both slightly higher than those obtained for the blank solution.

The polarization curves obtained for carbon steel immersed in  $W_2$ , shown in Figure 6, were very similar to the curves obtained in  $W_1$ . Only the addition of MIT caused a decrease in the anodic and cathodic current densities without shift of  $E_{corr}$ ; the current densities observed with the addition of MI were quite similar to those obtained in its absence (blank solution).

### 3.3.4. Surface characterization

Figure 7 shows SEM micrographs of carbon steel immersed for 24 hours in the  $CO_2$ -saturated produced water solution  $W_1$  in the absence and presence of MI and MIT. The morphology in Figure 7A shows that in the absence of inhibitors the surface was greatly damaged, creating a rough surface corresponding to uniform corrosion as previously reported [38]. The surface exposed to the solution containing MI (Figure 7B) was quite similar to that of the blank solution. The least-damaged metallic surface was that exposed to the MIT inhibitor solution (Figure 7C).

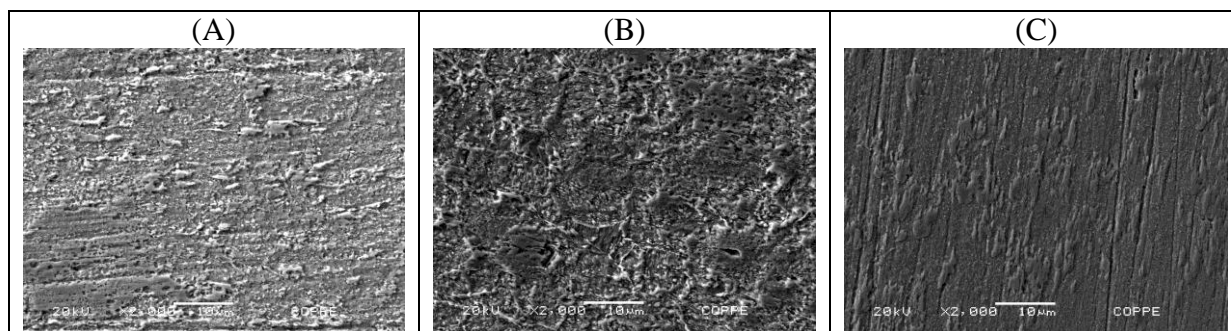


**Figure 7.** SEM images of corroded carbon steel surfaces after immersion in simulated produced water,  $W_1$ , in the absence (A) and presence of MI (B) and MIT (C).

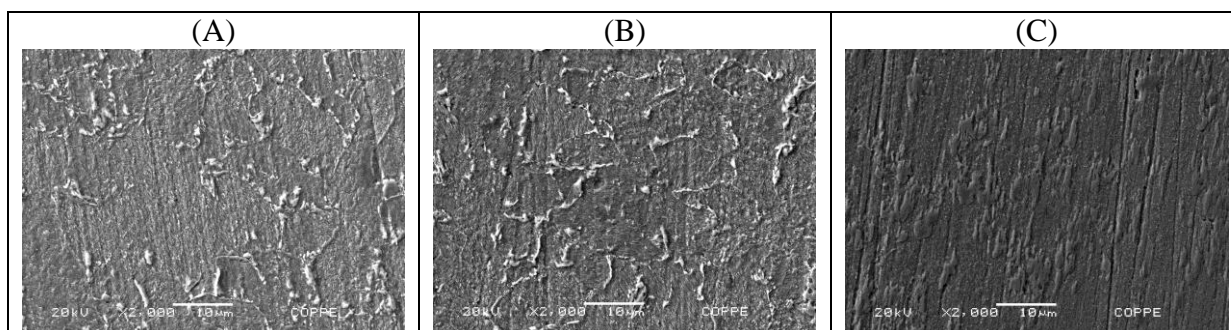


**Figure 8.** SEM images of corroded carbon steel surfaces after immersion in simulated produced water,  $W_2$ , in the absence (A) and presence of MI (B) and MIT (C).

SEM micrographs of carbon steel after immersion in the produced water solution W<sub>2</sub> (Figure 8) revealed results similar to those reported for W<sub>1</sub>. The MI-containing solution generated a rough surface (Figure 8B) similar to that of the blank solution. Only MIT's presence left a smooth surface, seen in Figure 8C. These results corroborate the electrochemical and weight loss measurement findings.

## 5. CONCLUSIONS

The following conclusions can be drawn from the above results:

- The simulated produced water solution W<sub>1</sub> showed lower corrosion rates than the simulated produced water solution W<sub>2</sub> although it is more acidic and has greater chloride content;
- Weight loss measurements and electrochemical analysis showed that of the isatin-derived compounds evaluated, only *N*-morpholine-3-isatin-thiosemicarbazone (MIT) acted as a corrosion inhibitor for carbon steel immersed in both the CO<sub>2</sub>-saturated simulated produced water solutions created;
- EIS results agree with the corrosion mechanism accepted in the literature, which involves iron electrochemical dissolution with an adsorbed intermediary species, FeOH<sub>ads</sub>;
- EIS results also showed a capacitive semicircle in the low-frequency range, associated with scale formation (FeCO<sub>3</sub>), but only for carbon steel immersed in the W<sub>2</sub> solution, suggesting a minimum bicarbonate (HCO<sub>3</sub><sup>-</sup>) concentration is needed for formation;
- The SEM images corroborated the electrochemical and weight loss measurements, showing that only *N*-morpholine-3-isatin-thiosemicarbazone acted as a carbon steel corrosion inhibitor.

## ACKNOWLEDGMENTS

The authors thank CNPq and PETROBRAS for their financial support.

## References

1. F. Ahmadun, A. Pendashteh, L. C. Abdullah, D. R. A. Biak, S. S. Madaeni, Z. Z. Abidin, *J. Hazard. Mater.* 170 (2009) 530.
2. X. Zhang, F. Wang, Y. He, Y. Du, *Corros. Sci.* 43 (2001) 1417.
3. D.M. Ortega-Toledo, J.G. Gonzalez-Rodriguez, M. Casales, M. A. Neri-Florez, A. Martinez-Villafane, *Mater. Chem. Phys.* 122 (2010) 485.
4. M. A. Deyab, *Corros. Sci.* 49 (2007) 2315.
5. A. M. Alsaabagh, M. A. Migahed, H. S. Awad, *Corros. Sci.* 48 (2006) 813.
6. H. Ashassi-Sorkhabi, S. A. Nabavi-Armi, *Electrochim. Acta* 47 (2002) 2239.
7. F. Farelas, A. Ramirez, *Int. J. Electrochem. Sci.* 5 (2010) 797.
8. Y. P. Khodyrev, E. S. Batyeva, E. K. Badeeva, E. V. Platova, L. Tiwari, O. G. Sinyashin, *Corros. Sci.* 53 (2011) 976.
9. D.M. Ortega-Toledo, J.G. Gonzalez-Rodriguez, M. Casales, A. Cacaes, L. Martinez, *Int. J. Electrochem. Sci.* 6 (2011) 778.
10. G. Zhang, C. Chen, M. Lu, C. Chai, Y. Wu, *Mater. Chem. Phys.* 105 (2007) 331.
11. M. H. Mohd, J. K. Paik, *Corros. Sci.* 67 (2013) 130.
12. D. Pinder, *Ocean and Coastal Management* .44 (2001) 579.

13. C. C. D. Henriques, C. J. B. M. Joia, I. P. Baptista, F. M. F. Guedes, *Offshore Technology Conference*, paper 23320, OTC, Houston, 2012.
14. M. A. Migahed, *Progress Organic Coatings* 54 (2005) 91.
15. M. A. Migahed, A. A. Farag, S. M. Elsaed, R. Kamal, M. Mostfa, H. Abd El-Bary, *Mater. Chem. Phys.* 125 (2011) 125.
16. X. Jiang, Y. G. Zheng, D. R. Qu, W. Ke, *Corros. Sci.* 48 (2006) 3091.
17. J. F. M. da Silva, S. J. Garden, A. C. Pinto, *J. Braz. Chem. Soc.* 12 (2001) 273.
18. D.D. N. Singh, M. M. Singh, R. S. Chaudhary, C.V. Agarwal, *J. Appl. Electrochem.* 10 (1980) 587.
19. G. Quartarone, T. Bellomi, A. Zingales, *Corros. Sci.* 45 (2003) 715.
20. Y. F. Barakat, A. M. Hassan, A. M. Baraka, *Mater. Sci. and Eng. Techn.* 31 (2000) 175.
21. A. A. Esmaili; S. Amini, A. Bodaghi, *Synllet*, 9 (2007) 1452.
22. L. Zhou, Y. Liu, W. Zhang, P. Wei, C. Huang, J. Pei, Y. Yuan, L. Lai, *J. Med. Chem.*, 49 (2006) 3440.
23. ASTM practice standard G-31 "Standard practice for laboratory immersion corrosion testing of metals", *ASTM International*, 2004.
24. ASTM practice standard G-1 "Standard practice for preparing, cleaning and evaluating corrosion test specimens", *ASTM International*, 2003.
25. R. Ketrane, B. Saidani, O. Gil, L. Leleyter, F. Baraud, *Desalination* 249 (2009) 1397.
26. V. S. Sastri, *Corrosion Inhibitors: Principles and Applications*, John Wiley & Sons, New York, 1998, 646.
27. J. B. Sun, G. A. Zhang, W. Liu, M. X. Lu, *Corros. Sci.* 57 (2012) 131.
28. G. Zhang, M. Lu, C. Chai, Y. Wu, *J. Univ. Sci. Techn. Beijing*, 13 (2006) 44.
29. J. Han, J. Zhang, J. W. Carey, *Int. J. Greenhouse Gas Control* 5 (2011) 1680.
30. D. A. López, S. N. Simison, S. R. de Sánchez, *Corros. Sci.* 47 (2005) 735.
31. E. C. French, R. L. Martin, J. A. Dougherty, *Materials Performance* 28 (1989) 46.
32. G.A. Zhang, Y. F. Cheng, *Corros. Sci.* 51 (2009) 87.
33. J.O. M. Bockris, D. Drazic, A. R. Despic, *Electrochim. Acta* 4 (1961) 325.
34. F. Farelas, M. Galicia, B. Brown, S. Nestic, H. Cataneda, *Corros. Sci.* 52 (2010) 509.
35. X. P. Guo, Y. Tomoe, *Corros. Sci.* 41 (1999) 1391.
36. D. H. Davies, G. T. Burstein, *Corrosion* 36 (1980) 417.
37. C. Cao, *Corros. Sci.* 38 (1996) 2073.
38. P. C. Okafor, X. Liu, Y. G. Zheng, *Corros. Sci.* 51 (2009) 761.